AIAA JOURNAL
Vol. 48, No. 7, July 2010

Unsteady Separation Control on Wind Turbine Blades Using Fluidic Oscillators

Ciro Cerretelli*
General Electric Global Research Europe, 85748 Munich, Germany
Werner Wuerz†
University of Stuttgart, 70049 Stuttgart, Germany
and
Emad Gharaibah‡
General Electric Global Research Europe, 85748 Munich, Germany

DOI: 10.2514/1.42836

Fluidic oscillators are actuators that are essentially constituted of a flow vane with no moving parts. They are very effective in generating an oscillating velocity field, and because of their robustness and potential to meet most application requirements they have been thoroughly investigated in previous years. In this work fluidic oscillators have been embedded in an airfoil representative of the outboard sections of wind turbine blades, and subsequently tested at full-scale Reynolds numbers $2.0 \cdot 10^6 \leq Re \leq 4.8 \cdot 10^6$ in the laminar wind tunnel at the University of Stuttgart. The effects of the unsteady actuation on the lift and drag strongly depend upon *Re*, the level of actuation, and the state of the airfoil surface. However, strong improvements have been obtained throughout the whole testing envelope, with relative lift increase spanning from a minimum of 10 to over 60% and substantial stall margin extension. In addition, employing fluidic oscillators strongly reduces the suction surface boundary-layer thickness and the unsteadiness of the mean flow velocity.

I. Introduction

THE drive toward the lowest possible cost of electricity (CoE) for wind turbines calls out for blade aerotechnologies that can be used to maximize the energy yield while minimizing cost, loads, and noise constraints. Aeroperformance is typically constrained by need to minimize extreme loads in off-design (parked or otherwise), which result from airfoil stall at high angles of attack. Separation and stall control via vortex generator jets, created by different actuators, either steady or unsteady pneumatic (i.e., pressurized air), or zero-net-mass flow-like synthetic jets or plasma actuators, is an enabling technology to overcome these limits on high-yield blade designs. With available separation control, blades with aggressive aerodynamic designs with low-solidity blades and/or operations at higher wind classes can become feasible.

Separation control via active flow control (AFC) is based on the injection of momentum in the retarded boundary layer; this results in the formation of vortices that entrain outer high-momentum fluid into the boundary layer, thereby delaying separation or even reattaching a separated flow. This has been an active area of development over the past couple of decades, and as more compact, powerful, and low system cost-flow control actuators are being developed, their application in industrial energy and propulsion systems has gathered growing interest. Given the potential for significant improvements in wind turbine performance, a technology program at General Electric Global Research studied the use of several actuation methods (pressure-fed and zero-net-mass flow) for steady and unsteady flow control; key results from an effort to validate the performance expected from the application of pneumatic oscillators for separation control are presented in this paper for real application Reynolds number ranging from $2 \cdot 10^6 \leq Re \leq 4.8 \cdot 10^6$. These validation experiments were conducted in collaboration with the Institute of Aerodynamics and Gas Dynamics at the University of Stuttgart.

Received 18 December 2008; revision received 29 November 2009; accepted for publication 2 December 2009.

*Currently Business Developer, Kiepe Electric, Milan, Italy; cirissimo@yahoo.com. Member AIAA.

†Research Scientist, Institute of Aerodynamics and Gas Dynamics; wuerz@iag.uni-stuttgart.de.

‡Research Scientist, Energy and Propulsion Technologies; emad.gharaibah@ge.com.

II. Unsteady Injection: Fluidic Oscillators for Flow Control

An extensive amount of research [1–5] has been performed in the last three decades on the development of a number of AFC technologies, typically with application to the separation delay or controlled reattachment of separated flows over lifting surfaces, to improve aerodynamic performance and extend the stall margin. A comprehensive review of flow control applications for several body shapes and generic airfoils is given by Wygnanski [6]. Unsteady blowing applied to flow control surfaces has been shown by many investigations to have potential for reducing flow separation and affecting the aerodynamic properties of surfaces. It is also very well known [7,8] that pulsing actuation in the boundary layer greatly reduces the amount of injected massflow that is necessary for the control of separation, therefore, a great deal of attention has been paid to the quantification of the benefits of pulsing [9]. Recent pulsed blowing implementations (referred to as pulsed vortex generator jets) have used pitched and/or skewed exhaust tubes to create specific vortical effects as the pulsed flow enters the cross stream [10]. A number of other experimental programs have used synthetic jets, zero-net-mass flux devices that consist of enclosed cavities where alternating periods of blowing and suction are created at an exhaust orifice by the time-periodic motion of a driver, which changes the volume of the cavity (among the numerous works see Amitay et al. [11,12]). Pulsed high-frequency plasma actuators have also been demonstrated using a pair of electrodes separated by a dielectric layer mounted on various flow control surfaces [13]. Combustion power actuators are currently also being developed [14].

Several challenges remain for the practical implementation of AFC technologies on full-scale airfoils. While it is relatively simple to develop successful actuators either for low Reynolds number wind-tunnel testing or for small-scale vehicles, it is clear that greater actuation power and high-speed actuator jets will be required to

maintain effectiveness at full scale with higher freestream velocities. Also, the majority of unsteady blowing actuators employ mechanical or piezoelectric devices that are often large in size, use numerous moving parts, have reliability issues and limited lifetime, or are extremely difficult to implement in harsh environmental conditions. For this reason, in recent years there has been a renewed interest in the field of fluidics [15].

Typical fluidic flow control actuators are employed to inject small amounts of air taken from high-pressure sources into the near-wall region upstream of a separated flow in a steady or unsteady fashion. In this way, the boundary layer may be sufficiently energized to overcome the downstream adverse pressure gradient and avoid flow separation. As the provision of this high-pressure air results in a penalty on the overall system performance, it is necessary to implement boundary-layer injection as efficiently as possible to maximize overall system benefits. Unsteady injection, being a more efficient streamwise vorticity production, offers one potential significant means of improving the energy balance, especially if the unsteadiness at a desired frequency can be achieved by purely passive means, i.e., without using valves or other powered devices. This injection mechanism can be obtained and perfected by employing fluidic oscillators. These fluidic actuators have the advantage of a high-frequency bandwidth, small mass flow requirements, and are essentially constituted of a flow circuit with no moving parts. For this reason, they have the potential to meet most application requirements. and there have been attempts [16] to incorporate these devices in turbomachinery components such as stator vanes. More recently, Cerretelli and Kirtley [17] have successfully demonstrated fluidic oscillators in a hump diffuser as means of preventing boundary-layer separation due to an adverse pressure gradient and have also proved substantial reductions in the amount of the actuator massflow that would be otherwise required by steady blowing. Cerretelli and Gharaibah [18] have shown how to employ lumped parameter analysis and computational fluid dynamics (CFD) methods to fine-tune these devices to the specific application.

A feedback oscillator constitutes the core of the no-moving-part actuator employed in this study. The working mechanism of such oscillators is shown in Fig. 1. This device consists of a high-gain bistable fluid amplifier, in which part of each output signal is fed back and applied as a negative signal at the amplifier's control port to switch the jet. The operation of the oscillator can thus be analyzed in two parts: the switching of the bistable amplifier, and the response of the feedback network. The switching time of the amplifier is typically negligible compared with the transport time of the network, therefore, the frequency of the oscillator is basically determined by the network itself.

To obtain the working equation for the oscillator, the lumped parameter analysis first described by Deadwyler [19] has been used. For the system described in Fig. 1 the feedback network can be modeled as an R–C–R equivalent circuit (see Fig. 2) where the mass flow m_1 is given in the feedback line, the entrance and exit orifices in the feedback volumes act as resistors (R_1, R_2), and the feedback volumes act as capacitors. A fluid resistor and capacitor can be written as:

$$R = \frac{\text{potential}}{\text{flow}} = \frac{\Delta P/\rho}{\dot{m}} \tag{1}$$

$$C = \frac{V\rho}{\gamma RT} \tag{2}$$

where ΔP is the pressure drop, ρ is the density, $\dot{m}$ is the mass flow, V is the capacitor volume, T is the temperature, γ is the polytrophic coefficient, and R is the gas constant. For a bistable fluid amplifier the switching of the power jet occurs when the differential flow across the power jet at the control nozzles reaches a critical value $\Delta\dot{m}_S = \dot{m}_{S1} - \dot{m}_{S2}$, where $\dot{m}_{S1}$ and $\dot{m}_{S2}$ are the mass flow at the switch-enacting branch and receiving branch, respectively. When the jet is flowing in the left outlet and will eventually switch to the right outlet, the differential flow can be computed as the rising control flow from the left feedback L minus the decaying control flow from the right feedback R, which can be written as:

$$\dot{m}_L = \frac{\Delta P}{(R_1+R_2)\rho}\left[1 - e^{-\left[\frac{R_1+R_2}{R_1R_2C}\right]t}\right] + \dot{m}_{S2}e^{-\left[\frac{R_1+R_2}{R_1R_2C}\right]t}$$
$$\dot{m}_R = \dot{m}_{S1}e^{-\left[\frac{R_1+R_2}{R_1R_2C}\right]t} \tag{3}$$

The difference flow for the network can thus be easily obtained as $\Delta\dot{m} = \dot{m}_L - \dot{m}_R$, which yields the following operating equation:

$$\Delta\dot{m} = \frac{\Delta P}{(R_1+R_2)\rho} - \left[\frac{\Delta P}{(R_1+R_2)\rho} + \Delta\dot{m}_S\right]e^{-\left[\frac{R_1+R_2}{R_1R_2C}\right]t} \tag{4}$$

Switching occurs when the differential flow reaches the critical value $\Delta\dot{m}_S$, and the switching time t_S can then be obtained from Eq. (4) when $\Delta\dot{m} = \Delta\dot{m}_S$. Because the switching process from right to left outlets is exactly identical, the full period of the oscillator will be twice the switching time and the frequency of oscillation is then given by:

$$f = \frac{1}{2t_S} = \frac{1}{2\frac{R_1R_2C}{R_1+R_2}\ln\left(\frac{\frac{\Delta P}{(R_1+R_2)\rho} + \Delta\dot{m}_S}{\frac{\Delta P}{(R_1+R_2)\rho} - \Delta\dot{m}_S}\right)} \tag{5}$$

From Eq. (5) it is possible to determine the necessary geometrical parameters to obtain the desired frequency, which are feedback volume, orifices, and length. As shown in a previous work by Cerretelli and Gharaibah [18], it is indeed possible to design fluidic oscillators that are pressure insensitive, and fluidic oscillators that are pressure controlled. Depending on the particular application, one of these two solutions would be preferred. For this study, it is advisable to operate at constant frequency of actuation to actuate at the point of maximum effectiveness, which, following results obtained in previous studies of this research program [17], should be tuned to comply to the $F^+ \sim 1$ criterion, defined by:

$$F^+ = \frac{f_e X_{\text{sep}}}{V_\infty} \tag{6}$$

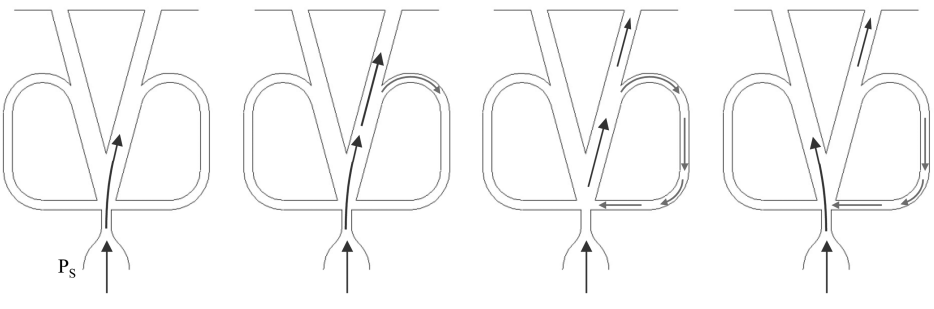

Fig. 1 Feedback fluidic oscillator: switching mechanism. P_S indicates the supply plenum pressure.

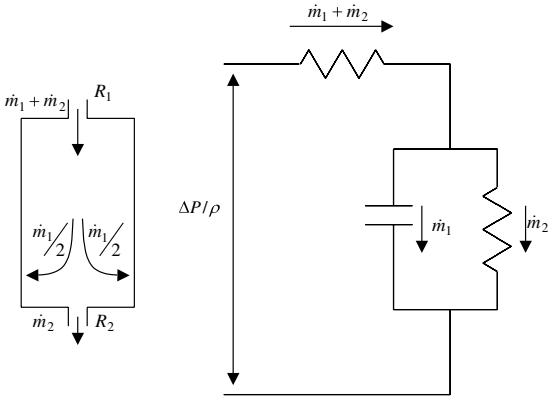

Fig. 2 R–C–R fluidic network.

where f_e = actuation frequency and X_{sep} is the separation length. This mode of operation also allows to evaluate the effectiveness of the actuators for different levels of mass flow independently of the frequency of actuation.

III. Pressure-Insensitive Unsteady Actuation

Using the lumped parameter analysis developed by the authors and following the theoretical and practical considerations discussed above, a feedback oscillator has been designed for our experiments, whereby the feedback path geometry is such that the device operates at a constant frequency f_e. Examples of the unsteady velocity waveforms measured with a hot-wire anemometer at the output of the oscillators are given in Fig. 3, together with the frequency response curve as a function of the driving pressure. The hot-wire probe was placed one nozzle diameter downstream of the exit surface. The modulation is very strong, with the rms velocity component ranging from 35 to 60% of the average value of the outlet velocity, as shown in Fig. 4.

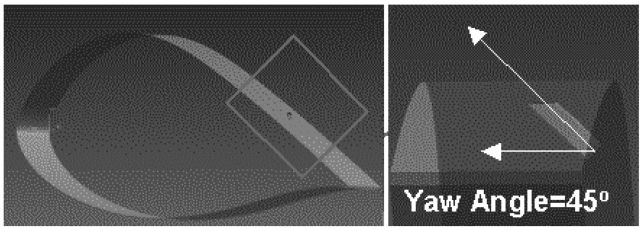

Fig. 5 Proof-of-concept 3D CFD simulations of AFC for separation control, with a depiction of the jaw angle (in this case, 45 deg).

It is somewhat difficult to quantify the pressure drop and the efficiency of a fluidic oscillator, because it is an unsteady device and it requires a pressure ratio significantly greater than 1 to operate in the bistable mode. An ideal oscillator would have a maximum velocity equal to the ideal frictionless velocity, a minimum velocity equal to zero (complete shutoff), and an rms velocity component of $1/\sqrt{2}$ of the average value. In practice, oscillators can never attain complete shutoff because of the inherent leakage that is present in any fluidic bistable switch. Figure 4 gives an indication of the efficiency of the oscillators employed in this work, by plotting the velocity of an ideal frictionless nozzle, the maximum velocity and the minimum velocity from the oscillator outlets. It can be noticed that the devices have a relatively small minimum velocity and the maximum velocities often exceed 80% of the ideal values.

IV. Design of Flow-Controlled Airfoil

The results presented here demonstrate the design of a flow control scheme for the DU-96 18% thick airfoil; it is a good representative airfoil for outboard sections of wind turbine blades and has been

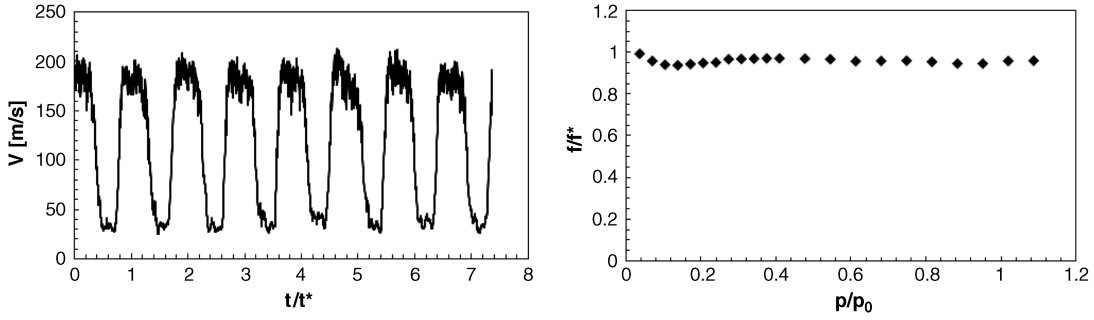

Fig. 3 Feedback fluidic oscillator: a) velocity waveform as measured by the HWA, and b) frequency response as a function of supply pressure.

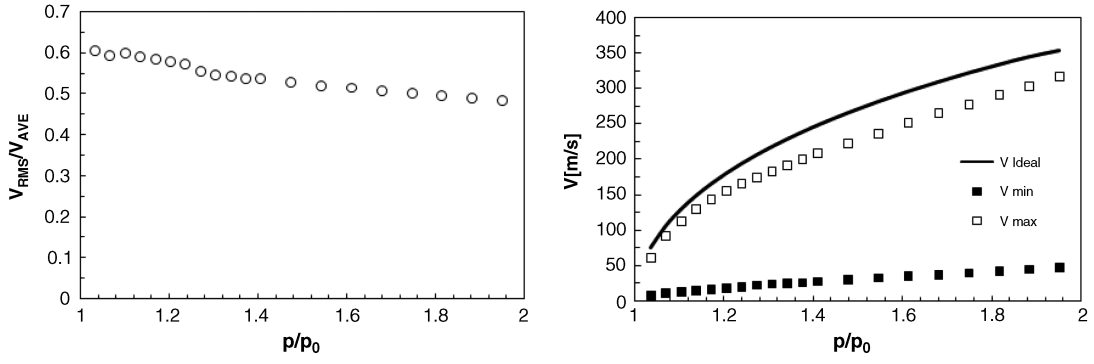

Fig. 4 a) RMS velocity component for the oscillator, and b) frictionless nozzle velocity, oscillator maximum, and minimum velocity as a function of the supply pressure.

Table 1 *Xs* and their ranges used in the screening design of experiment study. VR is the velocity ratio between the jet and freestream (VR $= V_j/V_\infty$). The levels are the number of intervals used in the design of experiment study within the specified range in this table

X	Range	Levels
Jet yaw angle, deg	30–45	3
Velocity ratio	1–2.5	3
Jet diameter, mm	3–6	2
Spacing	5–15diameter	3

tested exhaustively by General Electric Company and others. The design point chosen to represent a partially separated condition was an angle of attack of 12 deg at a freestream $V_\infty = 74$ m/s (that corresponds to a near-full-scale Reynolds number of 4 million), with the vortex generator jets installed at 72% chord.

In previous work at General Electric Global Research, CFD best practices for the use of the in-house CFD code (TACOMA) and the commercial CFX code to predict AFC effectiveness were developed and validated using data from internal experiments and the NASA Langley Research Center Flow Control Prediction Workshop. Optimization of jet location, strength, and characteristics was first conducted using 2D simulations. With guidelines from the 2D work, a screening designed experiment of 3D unsteady CFD analyses of 12 injector configurations (Fig. 5) was executed. The design variables *Xs* and their ranges used for the design study are summarized in Table 1.

To simulate the unsteady actuators efficiently, their internal workings were ignored and their simplified output modeled by a square, constant cross-section area injector. This jet forms a parallelogram jet-exit-shape by intersecting the airfoil surface, whose dimensions and the shape depend on the yaw and pitch angle of the jet. The cross section of the modeled injector was chosen to be equivalent to the area of a circular cross-section jet of the actuator that was going to be tested. Previous sensitivity studies had indicated that for this specific application, the hole shape detail is not a significant factor. These structured mesh sizes ranged from 2–9 million computation cells depending on the jet diameter and the span considered. The mesh in the injection region was refined (Fig. 6) to capture the jet's interactions with the mean flow accurately, spanwise as well as chordwise, and especially downstream of the injection holes and in the expected path of the jet flow. Y^+ values for all computational meshes used were of the order of unity to allow for integration to the wall in conjunction with the shear stress transport turbulence model [20]. Time steps were chosen short enough ($\sim$10e-5 [s]) to resolve the velocity oscillation (cycle duration $\sim$4e-3 [s]) of the actuators sufficiently. The actuation itself is modeled by imposing a velocity normal to the actuator boundary surface:

$$V_j = 2.5 \cdot \mathrm{VR} \cdot V_\infty \sin(2\pi \cdot f_j \cdot t) \tag{7}$$

where VR is the velocity ratio (VR $= V_j/V_\infty$), V_∞ is the freestream velocity, f is the frequency of the jet, and t is the time.

While the CFD studies indicated an optimal design of diameter 6 mm inclined with yaw angle of 30 deg and a pitch of 30 deg, an available oscillator design (from higher speed turbomachinery applications) could only be scaled up to 3 mm diameter and still meet the desired frequency to actuate unsteadiness based on an $F^+ \sim 1$ criterion; the associated volumetric packaging constraints also forced the design into a staggered hole configuration, as seen in Figs. 7 and 8. The final entitlement selected for testing was therefore somewhat unexpected, however, the freedom to go to higher velocity ratios (larger mass flows) in the test- cell was deemed to be sufficient to characterize the performance of this actuation system to its fullest extent.

For the fluidic oscillator, the final recommendation for the execution of the experiment was the configuration with: 3 mm hole,

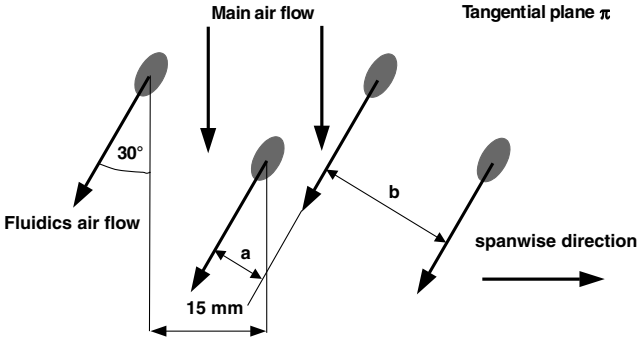

Fig. 8 Stacked arrangement for the oscillator jet exit nozzles.

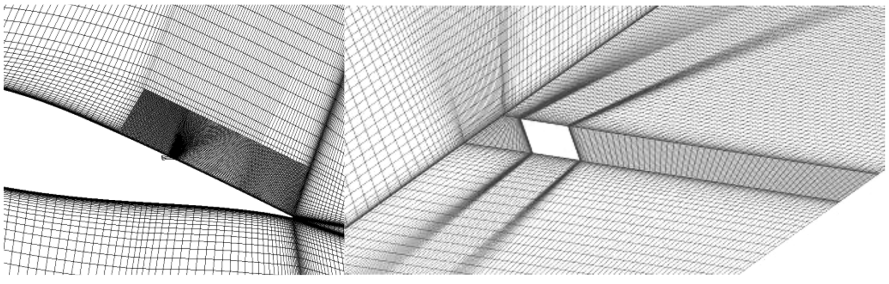

Fig. 6 Grid distributions used to capture near-wall boundary layers and jet flow.

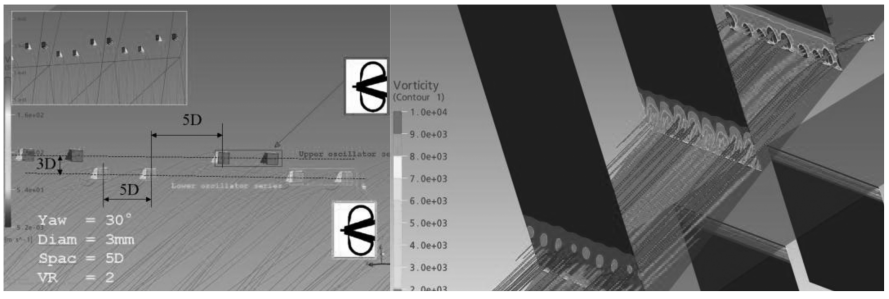

Fig. 7 Closeup of the CFD model for the fluidic oscillator, and streamwise vorticity production.

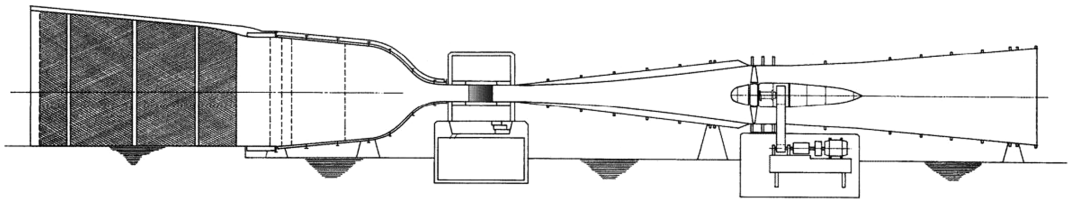

Fig. 9 Schematic of the laminar wind tunnel; total length is 46 m.

30 deg yaw, 30 deg pitch, and 5 diameter interhole spacing. An injection velocity ratio of 2 was predicted by CFD to provide about a 16.6% improvement in C_L. Preliminary test runs were performed with an airfoil section without actuator. The flow visualizations showed that turbulent separation at maximum lift started at around 68%, before the intended injector position, which was set at 72% chord. Therefore, in the experimental setup, the location of the injectors was changed to the 60% chord position.

V. Experimental Setup

The tests were performed in the laminar wind tunnel (LWT) of the Institute of Aerodynamics and Gas Dynamics at the University of Stuttgart. The LWT is an open-return tunnel with a closed test section (Fig. 9). The rectangular test section measures $0.73 \cdot 2.73$ m^2 and is 3.15 m long. A 2D airfoil model spans the short distance of the test section and gaps between model and tunnel walls are sealed.

Fig. 10 Picture of the DU96 airfoil in the laminar wind tunnel.

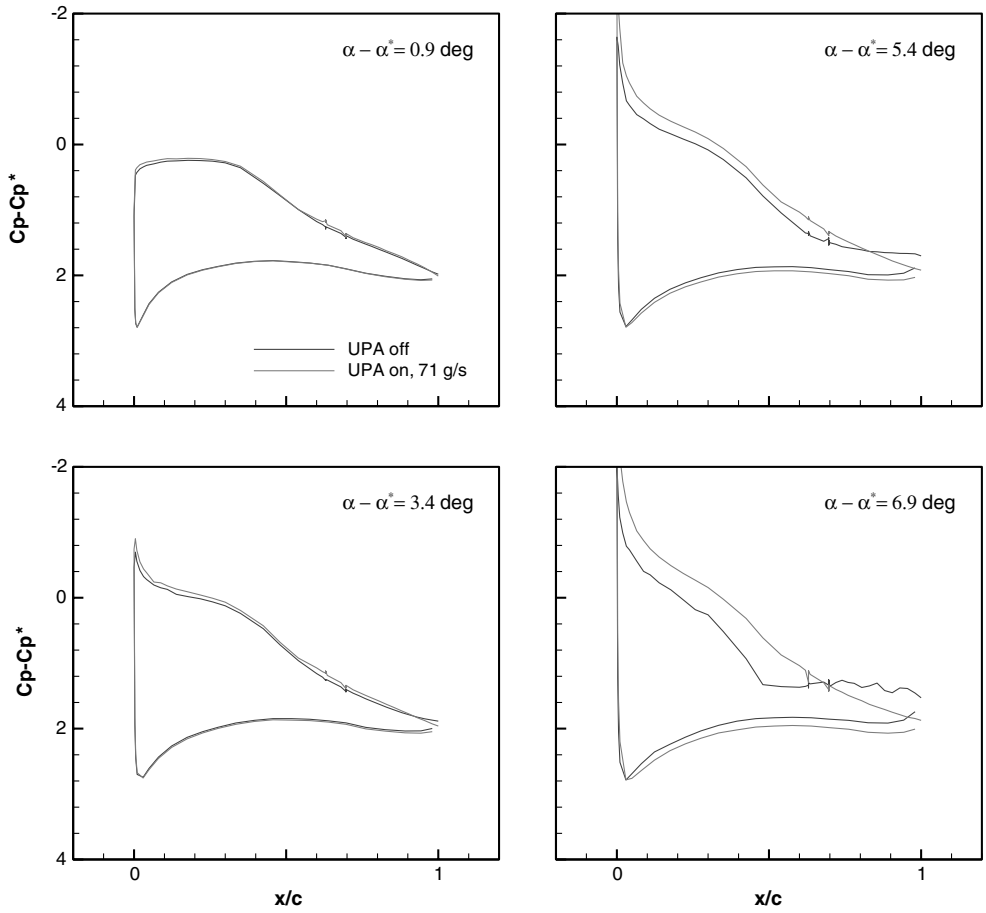

Fig. 11 Evolution of the airfoil C_p distribution at $Re = 4 \cdot 10^6$ for high UPAs on a smooth airfoil. The symbol $*$ indicates a reference state. Mass flow rates are to be intended as total rates for the entire span of actuators.

Figure 10 shows a picture of the airfoil (chord length $c = 0.8$ m) in the test section, with the actuator jet holes on the surface. The high contraction ratio of 100:1, as well as five screens and filters, results in a very low turbulence level of less than $Tu = \sqrt{\bar{u}'^2}/U_\infty = 2 \cdot 10^{-4}$ for a frequency range of 20–5000 Hz and a flow velocity of 30 m/s. Blowing air tangential in the corners between the model and the mounting plates is used as a boundary-layer control to ensure two-dimensional conditions. The nozzles were placed on the tunnel wall at $0.6\,x/c$ of the upper surface of the airfoil. For the present test setup the influence of the blowing was found to be quite small, which indicates that only minor flow separation takes place in the corners.

The lift is determined by experimental integration of the pressure distribution along the opposite two tunnel walls. The difference of both averaged pressures is proportional to the lift. In comparison to measurements with a balance, it is possible to avoid any gap between model and wind-tunnel wall. This is very important, especially for

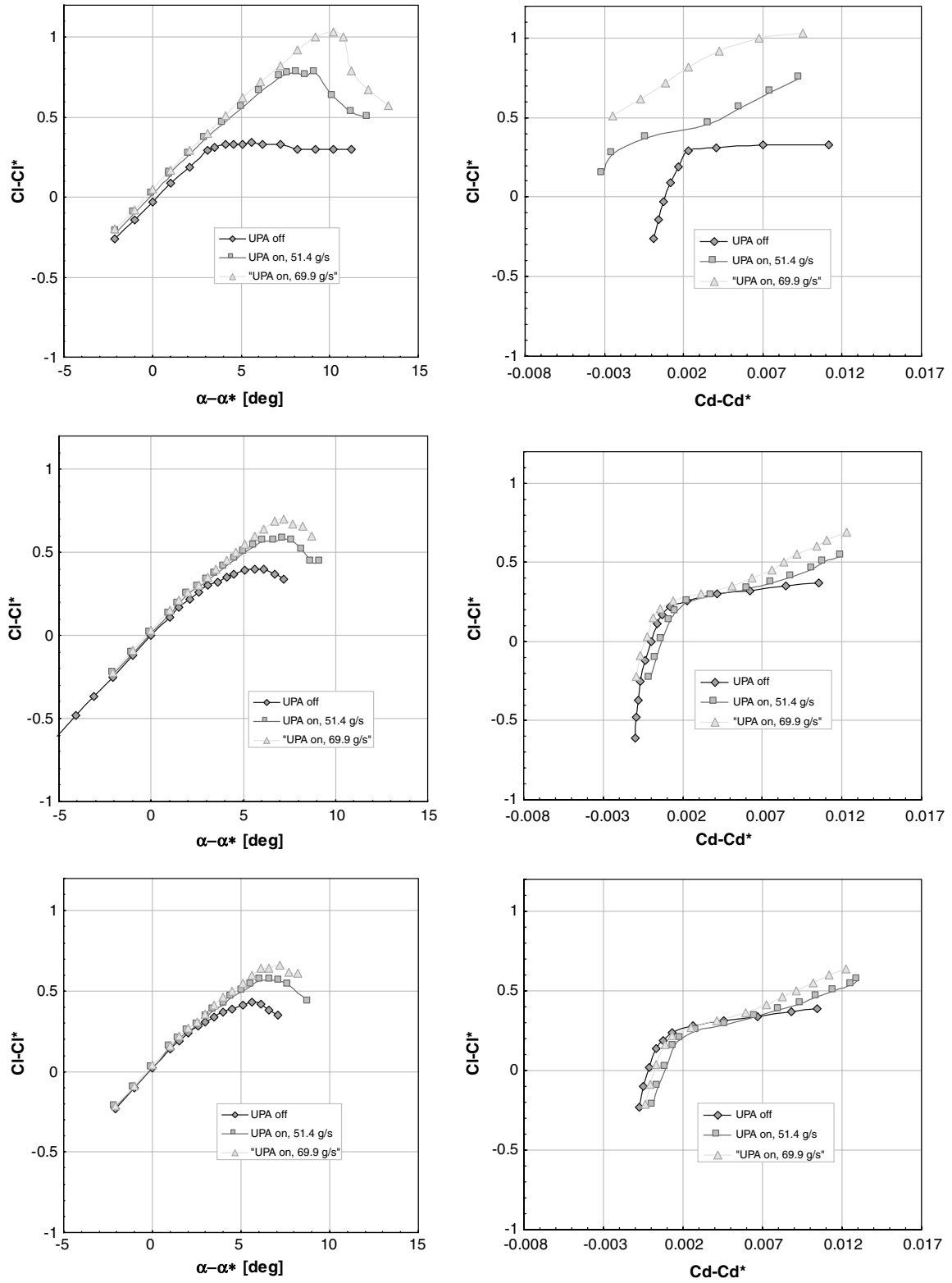

Fig. 12 UPA System—Polar Curves for smooth airfoil—from top to bottom—for (a) $Re = 2 \cdot 10^6$, (b) $Re = 4 \cdot 10^6$ and (c) $Re = 4.8 \cdot 10^6$. The symbol $*$ indicates a reference state. Mass flow rates are to be intended as total rates for the entire span of actuators.

high-lift systems. The drag is determined by an integrating wake rake, which is positioned approximately 0.35 chord length behind the model trailing edge. The rake automatically travels into the middle of the wake and adjusts itself parallel to the local flow direction. The width of the wake rake is selected according to the expected drag. For the actual tests, a standard wake rake with a width of 120 mm was used for the DU96. The pressure distributions of the DU96 sections were obtained by a Pressure Systems pressure scanning system. The C_p distributions were measured simultaneously with the normal polar measurements. Therefore, for every polar measurement point a pressure distribution is obtained. The experimental uncertainty on the lift and drag measurements is less than 1% [21].

Several measurements were performed with artificial roughness at the leading edge to simulate contamination of the rotor blade with

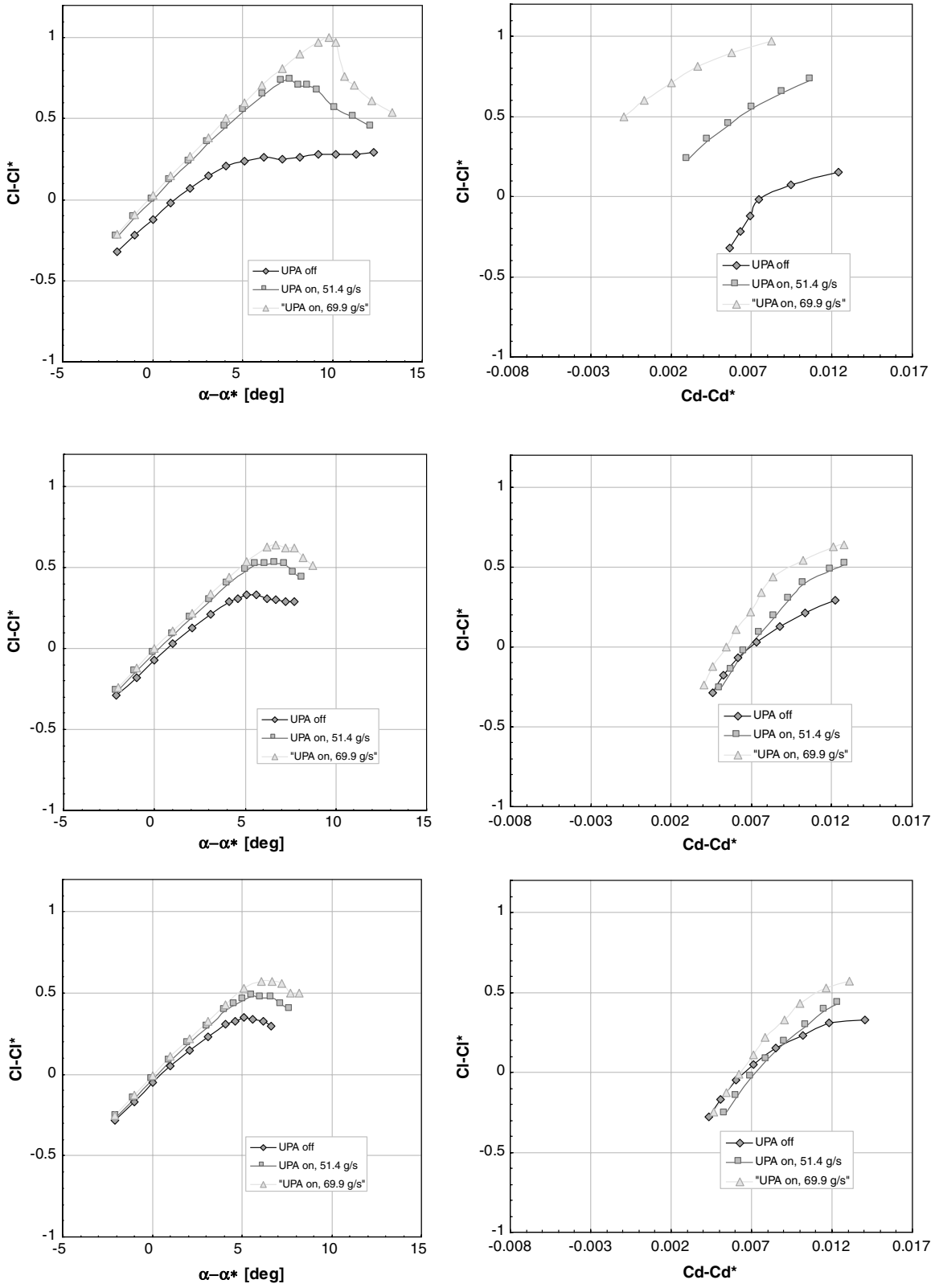

Fig. 13 UPA system: polar curves for rough airfoil (from top to bottom) for a) $Re = 2 \cdot 10^6$, b) $Re = 4 \cdot 10^6$, and c) $Re = 4.8 \cdot 10^6$. The symbol $*$ indicates a reference state. Mass flow rates are to be intended as total rates for the entire span of actuators.

insects. The roughness was produced from a very thin (d= 0.09 mm) bump tape with 10 mm width. The bumps are nearly half-circular and have a height of $h = 0.5$ mm. The spacing between the bumps was chosen to be 10 mm, and a total of seven tapes were mounted in a way to provide a staggered arrangement of the bumps.

To show the effect of the actuators on the boundary-layer development, it was decided to perform detailed wake traverses and spanwise scans using a single hot-wire probe. Measurements were performed for the clean case only (without the boundary-layer strip). The DISA 55P15 hot-wire probe was operated by a Dantec 55M10 bridge in constant temperature mode. The hot-wire was mounted on a sting downstream of the trailing edge and was fixed to the main traversing system of the wind tunnel.

VI. Effect of Flow Control on Lift, Drag for a Clean and Rough Airfoil

The effects of the unsteady pressure actuator (UPA) system on the airfoil pressure distribution and, therefore, on the airfoil lift and drag forces are illustrated in Fig. 11, which shows the evolution of the C_p distribution with the angle of attack at $Re = 4.0 \cdot 10^6$. At low AOA, the pressure distribution is basically unaffected by flow control, which produces very little change on the linear part of the C_l-α curve. It is not until $\alpha - \alpha^* = 3.4$ deg, when the flow on the suction side close to the trailing edge begins to separate, that significant changes in the pressure distribution can be noticed. In the stall region, where a large portion of the airfoil would normally undergo separation, the UPAs are able to keep the boundary layer attached, generating a significant difference in the pressure distribution, especially on the suction surface. This results in much higher values of lift. The significant increase in lift is further illustrated in Fig. 12, and it is substantial at all values of Re and levels of actuation. The maximum lift coefficient Cl is significantly higher, and the stall margin is also increased, because $\alpha_{Cl\mathrm{Max}}$ is higher and the curve remains smooth and gentle even in the poststall region. No hysteresis effects have been noticed in any of the wind-tunnel runs.

The effect of flow control on drag is dependent upon the Reynolds number and the actuation level. In principle, one can distinguish between two scenarios:

1) The flow is attached and the UPA can add momentum to the boundary layer, if the blowing rate in comparison to the velocities inside the boundary layer is large enough.

2) The flow is separated (without UPA), leading to large drag and a reduction in lift. Then the main effect of the UPA is its ability to keep the flow attached. While at $Re = 2.0 \cdot 10^6$ the UPA induces a substantial drag reduction, at $Re = 4.0 \cdot 10^6$ this occurs only at the highest levels of actuation, whereas the lower actuation level actually

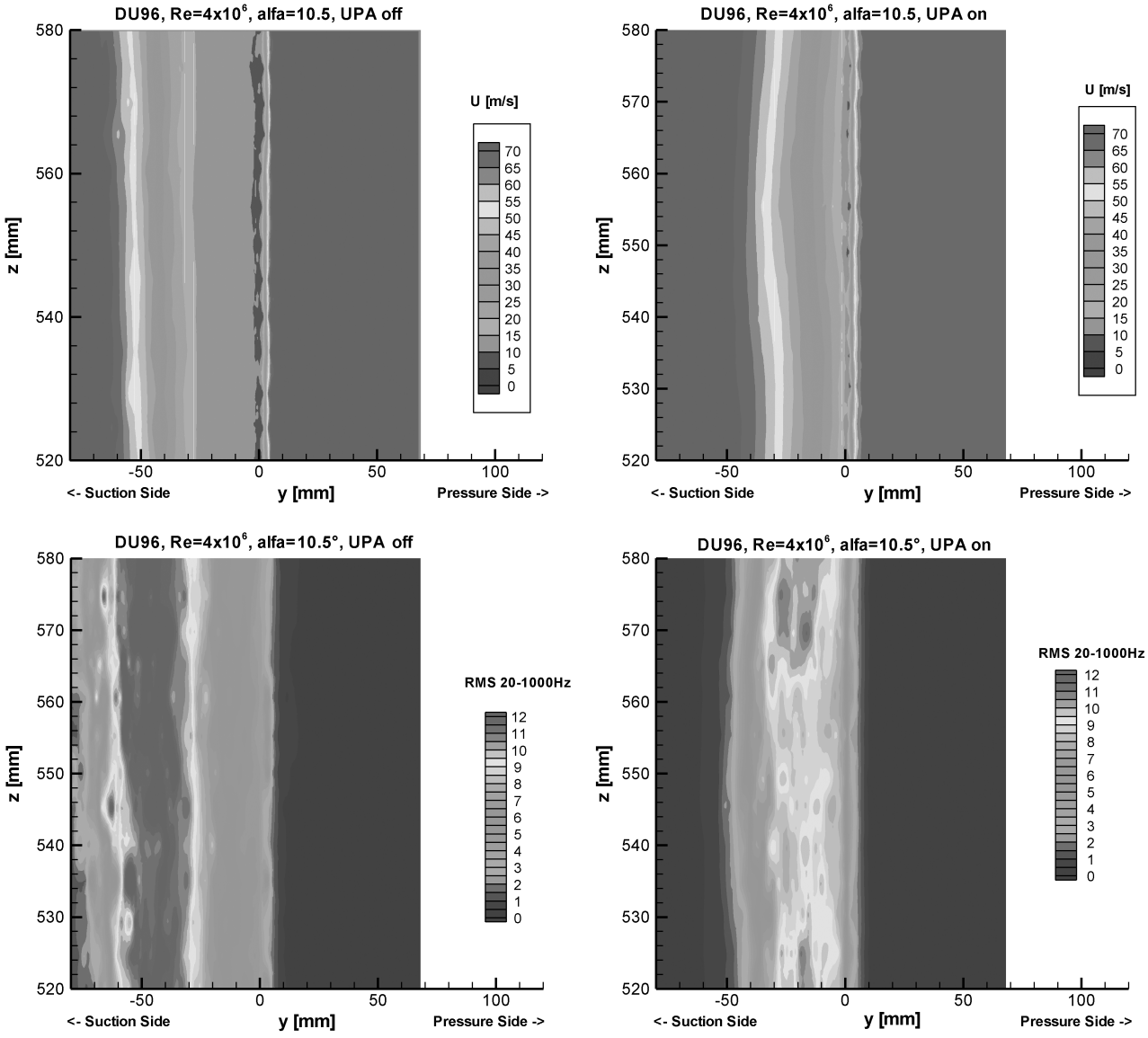

Fig. 14 UPA system: wake velocity and rms velocity measurements for $\alpha - \alpha^* = 5.4$ deg, $Re = 4 \cdot 10^6$.

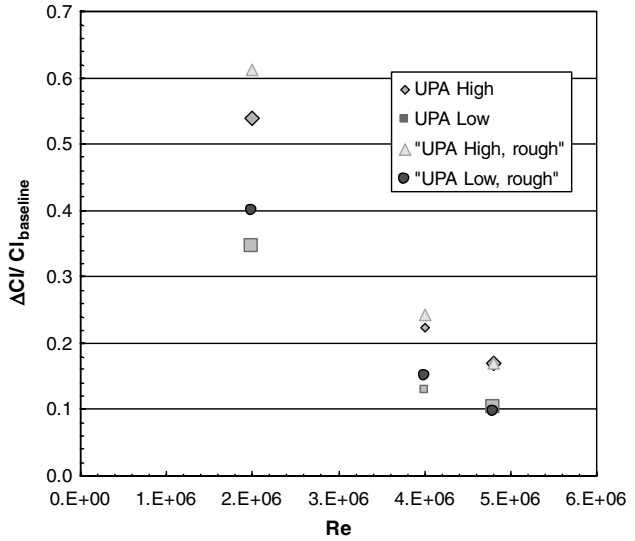

Fig. 15 Improvements in max C_L as a function of *Re* and velocity ratio for all tested configurations. High level of actuation refers to a mass flow of 69.9 g/s, and low level refers to a mass flow of 51.4 g/s.

slightly increases the drag in the region of the low-drag bucket of the polar. Nevertheless, in the stall area the drag reduction is seen again at both levels of actuation. This becomes the typical situation for the high Reynolds number case, where the UPA are able to reduce the drag only in the stall region because of the limited velocity ratio of the UPA system.

When roughness is applied at the leading edge of the airfoil, the benefits of flow control are demonstrated throughout the whole range of incidence. This is easily seen in Fig. 13 for the UPA system, as flow control shifts the linear part of the C_L-α curve upwards and the C_Ls increase remarkably even at lower angles of attack. Because of the long run of the turbulent boundary layer upstream of the UPA, the momentum close to the wall is already reduced when the main pressure rise starts. Here, the UPA system is able to balance this deficit, leading to a boundary layer with less tendency for separation.

The benefits on the drag are also stronger when roughness is present: the UPA consistently reduce the drag at all wind-tunnel speeds even in the lower range of angles of attack. The increase in maximum lift closer to the stall region is still present and as strong as for a smooth airfoil.

VII. Effect of Flow Control on the Airfoil Wake

Measurements of unsteady velocity have been performed with hot-wire traverses in the wake of the airfoil (3 mm downstream of the trailing edge) for two values of incidence, namely α-$\alpha^* = 1.4$ deg and α-$\alpha^* = 5.4$ deg. Figure 14 shows the contour plots on the velocity and rms velocity fields in the wake of the airfoil with and without flow control for α-$\alpha^* = 5.4$ deg, at which the upper side boundary layer would normally be separated, thus generating a very thick shear layer with a strong overall level of rms velocities. The wake measurements confirm the trends shown by the polar curves. The UPAs strongly reduce the suction surface boundary-layer thickness.

In addition, the unsteadiness of the mean flow velocity is reduced if the actuator is on. The mean velocity is increased close to the wall due to the actuator jets, and the boundary layer is a little bit thicker and shows a small waviness.

VIII. Conclusions

Fluidic UPAs have been used to apply unsteady boundary-layer injection on the separated flow of a typical wind turbine airfoil at full-scale Reynolds numbers. In the previous two decades, a great deal of attention has been paid to the quantification of the benefits of pulsing, and many authors have demonstrated successful applications with a variety of flow control applications for several body shapes and generic airfoils. The vast majority of these studies, however, generate unsteady blowing by means of mechanical or piezoelectric actuators that employ moving parts, have reliability issues and limited lifetime, and are difficult to implement at high temperatures.

The focus of the present effort is to demonstrate the viability of fluidic UPAs to perform unsteady blowing for wind turbine applications. These actuators essentially consist of a fluidic oscillator, have no moving parts or temperature limitations, and are therefore more attractive for implementation on production blades. To demonstrate the effectiveness of this unsteady injection technique, validation experiments have been conducted in collaboration with the Institute of Aerodynamic and Gas Dynamics at the University of Stuttgart. Polar curves have been measured for a wing section equipped with a staggered array of fluidic oscillators at $2 \cdot 10^6 \leq Re \leq 4.8 \cdot 10^6$, together with hot wire anemometer measurements in the wake.

The trends and results discussed in the previous sections are summarized in Fig. 15. The relative improvements in the lift coefficient are considerable, spanning from a minimum of 10% to over 60% depending upon the Reynolds number, upon the level of actuation, and the state of the airfoil surface. Reductions in drag occur at $Re = 2.0 \cdot 10^6$ for all actuation levels, while at $Re = 4.0 \cdot 10^6$ they occur only at the highest levels of actuation in the region of the low-drag bucket of the polar, because of the limited velocity ratio of the UPA system. Nevertheless, in the stall area the drag reduction is seen again for all levels of actuation. When roughness is applied on the airfoil surface, the benefits of flow control become stronger for both lift increase and drag reduction. In addition, the UPAs strongly reduce the suction surface boundary-layer thickness and the unsteadiness of the mean flow velocity. Such results are certainly encouraging for the engineer who is looking to successfully implement flow control in commercial products, in particular wind turbine airfoils.

Acknowledgments

General Electric Company's financial support is gratefully acknowledged. We have very much benefited from many discussions with Anurag Gupta, Georg Toplack, Kevin Kirtley, Stefan Herr, and Andreas Herrig.

References

[1] Lord, W. K., MacMartin, D. G., and Tillman, T. G., "Flow Control Opportunities in Gas Turbine Engines," AIAA Paper 2000-2234, 2000.
[2] Tilmann, C. P., Kimmel, R. L., Addington, G. A., and Myatt, J. H., "Flow Control Research and Applications at the AFRL's Air Vehicles Directorate," AIAA Paper 2004-2622.
[3] Lin, J. C., Howard, F. G., Bushnell, D. M., and Selby, G. V., "Investigation of Several Passive and Active Methods for Turbulent Flow Separation Control," AIAA Paper 1990-1598, 1990.
[4] Walker, S., "Lessons Learned in the Development of a National Cooperative Program," AIAA Paper 1997-3348, 1997.
[5] Anders, S. G., Sellers, W. L. III., and Washburn, A. E., "Active Flow Control Activities at NASA Langley," AIAA Paper 2004-2623.
[6] Wygnanski, I., "The Variables Affecting the Control of Separation by Periodic Excitation," AIAA Paper 2004-2505, 2004.
[7] Seifert, A., and Pack, L. G., "Active Control of Separated Flows on Generic Configurations at High Reynolds Numbers," AIAA Paper 99-3403, June–July 1999.
[8] Wygnanski, I., "Boundary Layer and Flow Control by Periodic Addition of Momentum," *4th AIAA Shear Flow Conference*, AIAA Paper 97-2117, June 29–July 2, 1997.
[9] Greenblatt, D., and Wygnanski, I., "The control of Flow Separation by periodic addition of momentum," *Progress in Aerospace Sciences*, Vol. 36, No. 7, 2000, pp. 487–545. doi:10.1016/S0376-0421(00)00008-7
[10] Magill, J., and McManus, K., "Control of Dynamic Stall Using Pulsed Vortex Generator Jets," AIAA Paper 98-0675, January 1998.
[11] Amitay, M., Smith, B. L., and Glezer, A., "Aerodynamic flow control using synthetic jet technology," AIAA Paper 98-0208, 1998.
[12] Amitay, M., Kibens, V., Parekh, D. E., and Glezer, A., "Flow reattachment dynamics over a thick airfoil controlled by synthetic jet actuators," AIAA Paper 99-1001, 1999.

[13] Wilkinson, S., "Investigation of an Oscillating Surface Plasma for Turbulent Drag Reduction," AIAA Paper 2003-1023, 2003.
[14] Crittenden, T. M., "Environmental Testing of Combustion Powered Actuators for Flow Control," AIAA Paper 2007-3855, 2007.
[15] Gregory, J., Sullivan, J., Raman, G., and Raghu, S., "Characterization of a Micro Fluidic Oscillator," *AIAA Journal*, Vol. 45, No. 3, pp. 568–576. doi:10.2514/1.26127
[16] Culley, D. E., Prahst, P. S., Bright, M. M., and Strazisar, A. J., "Active Flow Separation Control of a Stator Vane using Surface Injection in a Multistage Compressor Experiment," *Proceedings of ASME Turbo Expo*, American Society of Mechanical Engineers Paper GT2003-38863, 2003.
[17] Cerretelli, C. and Kirtley, K., "Boundary Layer Separation Control with Fluidic Oscillators," American Society of Mechanical Engineers Paper GT2006-90738, 2006.
[18] Cerretelli, C., and Gharaibah, E., "An Experimental and Numerical Investigation on Fluidic Oscillators For Flow Control," AIAA Paper 2207-3584.
[19] Deadwyler, R., "Theory of Temperature and Pressure Insensitive Fluid Oscillators," Harry Diamond Lab. TR 1422, 1969.
[20] Menter, F. R., "Two-Equation Eddy-Viscosity Turbulence Models for Engineering Applications," *AIAA Journal*, Vol. 32, No. 8, 1994, pp. 1598–1605. doi:10.2514/3.12149
[21] Würtz, W., Herrig, A., Vetter, C., and Langohr-Kolb, M., "Wind Tunnel Measurements of the B1-18 Airfoil Section with Active Flow Control Devices," *Wind Energy*, Wiley, Hoboken, NJ, 2006.

F. Coton
Associate Editor